Post-injury protective astrogenesis from SVZ niche is controlled by Notch modulator Thbs4

Eric J. Benner[1], **Dominic Luciano**[2,3], **Rebecca Jo**[1,2], **Khadar Abdi**[2], **Patricia Paez-Gonzalez**[2], **Huaxin Sheng**[4], **David Warner**[4], **Chunlei Liu**[5], **Cagla Eroglu**[2,6], and **Chay T. Kuo**[1,2,3,6,7]

[1]George and Jean Brumley Neonatal-Perinatal Research Institute, Department of Pediatrics, Duke University School of Medicine, Durham, NC 27710, USA

[2]Department of Cell Biology, Duke University School of Medicine, Durham, NC 27710, USA

[3]Department of Neurobiology, Duke University School of Medicine, Durham, NC 27710, USA

[4]Department of Anesthesiology, Duke University School of Medicine, Durham, NC 27710, USA

[5]Department of Radiology, Duke University School of Medicine, Durham, NC 27710, USA

[6]Duke Institute for Brain Sciences, Duke University School of Medicine, Durham, NC 27710, USA

[7]Preston Robert Tisch Brain Tumor Center, Duke University School of Medicine, Durham, NC 27710, USA

Abstract

Postnatal/adult neural stem cells (NSCs) within the rodent subventricular/subependymal zone (SVZ/SEZ) generate Doublecortin (DCX)$^+$ neuroblasts that migrate and integrate into olfactory bulb circuitry[1,2]. Continuous production of neuroblasts is controlled by SVZ microenvironmental niche[3,4]. It is generally believed that enhancing neurogenic activities of endogenous NSCs may provide needed therapeutic options for disease states and after brain injury. However, SVZ NSCs can also differentiate into astrocytes. It remains unclear if there are conditions that favor astrogenesis over neurogenesis in the SVZ niche, and if astrocytes produced there exhibit different properties from others in the brain. We have uncovered that SVZ-generated astrocytes express high levels of Thrombospondin-4 (Thbs4)[5,6], a secreted homopentameric glycoprotein, in contrast to cortical astrocytes which are Thbs4^{low}. We found that localized photothrombotic/ischemic cortical injury initiates a marked increase in Thbs4^{hi} astrocyte production from the postnatal SVZ

Correspondence: Chay T. Kuo, Departments of Cell Biology, Neurobiology, Pediatrics, Duke University School of Medicine, 366 Nanaline Duke Bldg. Box 3709, 307 Research Drive, Durham, NC 27710, chay.kuo@duke.edu.

niche. Tamoxifen-inducible *nestin-CreER^tm4* lineage-tracing demonstrated that it is these SVZ-generated Thbs4^{hi} astrocytes, and not DCX[+] neuroblasts, that home-in on the injured cortex. This robust post-injury astrogenic response required SVZ Notch activation, modulated by Thbs4 via direct Notch1 receptor binding and endocytosis to activate downstream signals, including increased Nfia transcription factor expression important for glia production[7]. Consequently, *Thbs4^KO/KO* animals showed severe defects in cortical injury-induced SVZ astrogenesis, instead producing cells expressing DCX from SVZ to the injury sites. These alterations in cellular responses resulted in abnormal glial scar formation after injury, and significantly increased microvascular hemorrhage into the brain parenchyma of *Thbs4^KO/KO* animals. Taken together, these findings have significant implications for post-injury applications of endogenous and transplanted NSCs in the therapeutic setting, as well as disease states where Thbs family members play important roles[8,9].

Keywords

subventricular zone; astrogenesis; brain injury; Thbs4; Notch; tsp

---

We want to understand neurogenesis/astrogenesis choice in the postnatal SVZ niche, and the cellular properties of SVZ-generated astrocytes. CNS astrocytes secrete Thrombospondins (Thbs), a family of homotrimeric and homopentameric proteins[6]: we asked whether SVZ-generated astrocytes express different Thbs protein(s) than their cortical counterparts. We started by establishing primary SVZ adherent cultures from *nestin-CreER^tm4 (N4); rosa26reporter-tdTomato (RTM)* animals, after postnatal day 7 (P7) tamoxifen injection. We showed previously that this *N4* line can inducibly and efficiently lineage-trace progeny of postnatal/adult SVZ NSCs[4,10] (Supplementary Fig. 1 and Mov. 1). Following 5 days of differentiation, tdTomato[+] lineage-traced GFAP[+] astrocytes showed strong immunohistochemical (IHC) staining for Thbs4 (Supplementary Fig. 2a). To confirm the specificity of this antibody staining, we performed the same culture experiment using *Thbs4^KO/KO* mutant animals[11], which revealed no Thbs4 immunofluorescence under identical experimental/imaging conditions (Supplementary Fig. 2b). Western blot analyses confirmed these findings (Supplementary Fig. 2c). Comparison of differentiated SVZ astrocyte cultures to primary astrocytes harvested from the cortex showed selective Thbs4 expression by SVZ astrocytes (Fig. 1a). This difference in Thbs4 expression was further demonstrated by quantitative PCR (qPCR) analyses of FACS-purified GFP[+] cortical vs. SVZ astrocytes from *GFAP-GFP* transgenic animals (Fig. 1b). IHC staining on P14 brain sections indicated that Thbs4, while co-labeling with SVZ GFAP[+] astrocytes, did not co-localize with Mash1^{+} transiently amplifying progenitors, DCX[+] neuroblasts, or NG2^{+}, Olig2^{+} populations in the SVZ niche (Supplementary Fig. 3a - e).

We next tested whether SVZ-generated GFAP[+] astrocytes are fated to express Thbs4 in vivo. We transplanted second passage SVZ NSC cultures harvested from tamoxifen-induced *N4; RTM* animals into the cerebral cortex of WT/non-transgenic animals (Fig. 1c). Unlike transplantations into the SVZ, which generated neuroblasts that migrate to the olfactory bulb[4,12] (Supplementary Fig. 4), tdTomato^{+} cells transplanted into the cortex after 2 to 4 weeks gave rise to GFAP[+]Thbs4^{hi} astrocytes, contrasting with resident cortical astrocytes

which were Thbs4^{low} (Fig. 1c). Of the 402 *N4* lineage-traced tdTomato$^+$ cells counted over multiple experiments, 96.8% (389) showed GFAP expression. Strong Thbs4$^+$ IHC co-staining was detected in 98.2% (382) of these GFAP$^+$ cells.

Next, we wondered under which conditions the SVZ niche favored Thbs4^{hi} astrocyte production. SVZ NSCs are thought to respond to middle cerebral artery occlusion-induced stroke by producing DCX$^+$ neuroblasts that migrate into the striatum[13]. Although some have also reported gliogenic responses after injury[14,15]. To generate precisely localized cortical injuries directly over the SVZ niche we used photothrombosis, a well-defined ischemic injury model[16] (Fig. 2a). We performed these injuries using *N4; RTM* animals after P6 tamoxifen injection: this timing allowed us to specifically target/lineage-trace SVZ NSCs, while minimizing Cre-reporter labeling of cortical cells[10]. We induced cortical injuries at P12 and examined the SVZ responses at 3 and 14 days post injury (dpi), using 3,3′-Diaminobenzidine (DAB) IHC staining against tdTomato, allowing simultaneous visualization of tdTomato-reporter expression and brain tissue histology. At 3 dpi, we did not see significant morphological changes to lineage-traced tdTomato$^+$ cells around the SVZ (Fig. 2b). However, by 14 dpi, we observed robust populations of tdTomato$^+$ cells between SVZ and cortical injury site (Fig. 2b). This delayed reaction was specific to SVZ/hemisphere ipsilateral to the injury, as we did not detect obvious changes to tdTomato$^+$ cells in the contralateral cortex, nor did we see changes in the ipsilateral cortex in sham-treated control brains (Supplementary Fig. 5a, b). As a further control, we did not detect tdTomato$^+$ cells in the injured cortex of *N4; RTM* animals without tamoxifen injection (Supplementary Fig. 5c). We also did not observe tdTomato$^+$ cells next to superficial cortical injuries, suggesting a correlation between injury severity and SVZ responses (data not shown). All analyses were performed on cortical injuries that did not breach the corpus callosum (determined by sectioning through the entire injured area), limiting potential spill-over of SVZ niche neuroblasts into the injured areas.

IHC staining showed that the majority of tdTomato$^+$ cells next to the injury site 14 dpi had complex morphologies, labeled strongly with anti-Thbs4 antibody, and co-stained with GFAP (Fig. 2c, d). Although we did not observe tdTomato$^+$ cells at the injury site 3 dpi, Western blotting and IHC staining of SVZ tissue showed that, at this early time point, the ipsilateral SVZ had upregulated Thbs4 expression as compared to the contralateral side (Fig. 2e, f). This Thbs4 expression remained localized to GFAP$^+$ astrocytes (Supplementary Fig. 3f). Repeating these injury experiments using the *GFAP-Cre* driver (JAX #004600) instead of *N4*, we observed similarly robust tdTomato$^+$ lineage-traced cells around the injury site 14 dpi (Supplementary Fig. 6). Though they likely represents a heterogeneous cell population, since the *GFAP-Cre* driver also efficiently lineage-traced cortical cells (Supplementary Fig. 6). To investigate whether cortical astrocytes can upregulate Thbs4 expression to levels seen in SVZ astrocytes after injury, we performed qPCR analyses 3 dpi on FACS-sorted GFP$^+$ cortical vs. SVZ astrocytes from *GFAP-GFP* animals (prior to significant migration from SVZ), which showed that SVZ astrocytes remained the Thbs4^{hi} population (Supplementary Fig. 7).

What are the molecular signals controlling this injury-induced Thbs4^{hi} astrogenesis from the SVZ? The Notch pathway is an important regulator of SVZ NSC and niche function[10,17], as

well as neurogenesis vs. gliogenesis choice[18]. To determine if Notch activation is required for Thbs4^{hi} astrocyte production after cortical injury, we inducibly deleted RBPJκ[19], the Notch Intra-Cellular Domain (NICD) co-transcriptional activator, using the *N4* transgene. We crossed *N4; RBPJκ[KO/+]* mice to *RTM[Flox/Flox]; RBPJκ[Flox/Flox]* mice and treated new mouse litters with tamoxifen at P6. We then compared lineage-traced tdTomato^{+} cells around the cortical injury site between *N4; RTM; RBPJκ[Flox/+]* (control) and *N4; RTM; RBPJκ[KO/Flox]* inducible mutant (iKO) animals at 14 dpi. DAB staining revealed that while there were robust tdTomato^{+} cells between the SVZ and cortical injury site in the controls (Fig. 3a), this response was blunted in *RBPJκ* iKO animals (Fig. 3a, b). We next asked if increased Notch signaling can result in enhancement of SVZ response after injury. Using *N4; RTM; rosa26r-NICD[Flox/+]* animals to over-express NICD in lineage-traced SVZ cells after tamoxifen injection, we repeated the cortical injury experiments. DAB staining 14 dpi showed significantly increased numbers of lineage-traced tdTomato^{+} cells at the injury site in NICD over-expressing animals (Fig. 3a, b). Consistent with these results, IHC staining of wild-type brain sections following cortical photothrombosis showed upregulated Notch1 receptor expression in the ipsilateral SVZ 2 dpi (Supplementary Fig. 8). And Western blot analyses 3 dpi revealed an increase in NICD protein in the ipsilateral SVZ (Fig. 3c).

Ependymal cells, labeled/lineage-traced by *FOXJ1*-based reporters/drivers, have been reported to respond to ischemic injury by generating progeny that migrate to the injury site[20]. Since this *N4* line also targets ependymal cells[4,10], thus potentially lineage-tracing ependymal progeny after injury, we performed identical cortical injuries in *FOXJ1-CreER[t2]; RTM* animals after P6 tamoxifen injection. In repeated experiments we did not observe migration of tdTomato[+] populations from SVZ to the cortical injury sites either early (3 dpi) or late (14 dpi) (Supplementary Fig. 9a and data not shown). The *FOXJ1-CreER[t2]* driver also labeled mature cortical neurons, but this expression was independent from injury-induced cell proliferation (Supplementary Fig. 9a and data not shown). To rule out the possibility that modification of Notch signaling allowed ependymal cells to generate progeny responding to injury, we performed cortical injury experiments in *RBPJκ* iKO and *rosa26r-NICD* over-expression backgrounds using the *FOXJ1-CreER[t2]* driver. In both genetic backgrounds we did not observe migration of tdTomato^{+} cells from SVZ to the injury sites (Supplementary Fig. 9b).

Thbs2 has been shown to physically interact with the Notch3 receptor in vitro[21]. Thus, we wondered if Thbs4 plays a direct role in modulating Notch activity after cortical injury. To test this, we first differentiated early passage SVZ NSC cultures in the presence of immobilized Jagged1-Fc. Since transient Notch activation is known to decrease neurogenesis[18], immobilized Jagged1-Fc resulted in decreased neuroblast production compared to untreated control cultures (Fig. 3d, f). We repeated this assay with the addition of recombinant Thbs4 alone in the medium, and observed a similarly robust decrease in neuroblast production (Fig. 3d, f). This was confirmed by Western blot analyses for DCX protein after 5 days of differentiation (Fig. 3e, f). DAPT or DBZ, common Notch pathway inhibitors, conversely increased production of neuroblasts from differentiating SVZ cultures (Supplementary Fig. 10 and data not shown). Thbs4 was unable to blunt DAPT or DBZ-

mediated effects (Supplementary Fig. 10), suggesting that Thbs4's function in this setting required Notch activity.

Since SVZ NSCs express the Notch1 receptor[17], we asked whether Thbs4 and Notch1 can physically interact. Using varied concentrations of purified Thbs4 protein and recombinant Notch1-Fc fragment (including the first 13 extracellular EGF-like repeats of Notch1), pull-down experiments showed direct Thbs4/Notch1-Fc interactions in vitro (Supplementary Fig. 11a). mIgG2a, an isotype-specific control for Notch1-Fc, as well as purified Thbs2 protein, did not show Notch1-FC interactions (Supplementary Fig. 11a). We next harvested cellular extracts from primary SVZ NSC cultures with or without addition of Thbs4 in the medium. Immunoprecipitation (IP) with anti-Notch1 antibody was able to pull-down Thbs4 from the culture lysates in the +Thbs4 condition (Supplementary Fig. 11b). While under physiological conditions, IP from freshly isolated SVZ tissues using anti-Notch1 antibody did not detect significant Thbs4 pull-down (Supplementary Fig. 11c), similar IP experiments 3 dpi revealed Notch1/Thbs4 interactions (Fig. 3g).

Efficient Notch signaling requires receptor-endocytosis into endosomes[22], and Thbs4 as a pentameric protein may promote Notch endocytosis and activation. To test this possibility, we cultured primary SVZ NSCs in the presence of both Thbs4 and late endocytosis blocker Dynasore. Addition of Thbs4 alone resulted in NICD upregulation, as detected by Western blotting 15 minutes after incubation, and lasting for several hours thereafter (Fig. 3h, Supplementary Fig. 11d). This NICD increase was blocked by Dynasore (Fig. 3h). By 36 hours after stimulation, Thbs4-induced NICD upregulation had subsided, and as expected with Dynasore added there was low NICD with or without Thbs4 in medium (Supplementary Fig. 11e). The transcription factor Nfia is an important regulator of gliogenesis downstream of Notch signaling[7,23]. Following Thbs4 addition during SVZ NSC differentiation in vitro, we detected increased Nfia expression over control conditions (Supplementary Fig. 11f). Similarly, Western blotting of SVZ tissues 3 dpi showed increased Nfia protein levels in the ipsilateral vs. contralateral SVZ (Fig. 3i), consistent with injury-induced SVZ astrogenic response (Fig. 2e, f).

Our findings raised the intriguing possibility that Thbs4, following cortical injury, is itself necessary for Notch-mediated SVZ astrogenesis. To test this, we first performed Western blot analyses on SVZ tissue from $Thbs4^{KO/KO}$ animals 3 dpi. While under physiological conditions we did not detect noticeable differences in SVZ NICD expression levels between $Thbs4^{KO/+}$ (control) and $Thbs4^{KO/KO}$ mutant animals (Supplementary Fig. 12a), these mutants lacked NICD increase in the ipsilateral SVZ 3 dpi (Fig. 4a) unlike WT animals (Fig. 3c). Further, $Thbs4^{KO/KO}$ animals did not show appreciable increase in Nfia expression in the ipsilateral SVZ 3 dpi (Fig. 4a). We next tamoxifen-induced $N4; RTM; Thbs4^{KO/KO}$ animals to lineage-trace responding SVZ-derived cells after cortical injury, according to the same protocol described above. At 14 dpi, the tdTomato+ cells around the injury site showed a surprising neuroblast-like morphology, and mostly co-labeled with DCX rather than GFAP (Fig. 4b, c, Supplementary Fig. 12b). This is in striking contrast to cortical injuries in control animals, where few DCX+ cells were detected next to the injury site (SVZ neuroblast staining was used as internal control for DCX antibody, Fig. 4c, Supplementary Fig. 13). The observed mixture of tdTomato- and tdTomato+ DCX+ cells at the cortical injury site is

consistent with the clonal nature of *N4*-mediated recombination following tamoxifen induction[4,10].

In preparing the injured brains from *Thbs4^{KO/KO}* animals, we noticed significant hemorrhage around the injured cortical areas. We next performed brain magnetic resonance imaging (MRI) analyses on control and *Thbs4^{KO/KO}* littermates. Using 3D structural MRI on brains inside intact skulls, we can identify the location and extent of cortical injuries (Supplementary Fig. 14a, b). In isotropic diffusion-weighted images, the boundaries of lesions were hyperintense in both control and *Thbs4^{KO/KO}* animals (Supplementary Fig. 14a, b), demonstrating classical characteristics of stroke infarct[24]. The interiors of these lesions appeared hypointense as result of increased edema, and quantitative maps of diffusion coefficients confirmed hindered molecular diffusion in the infarcted, but faster diffusion in the edematous areas (Supplementary Fig. 14a, b). We did not detect significant Mean Diffusivity measurement differences between littermate control and *Thbs4^{KO/KO}* animals in the infarcted or edematous cortical areas, either 2 dpi (data not shown) or 8 dpi (Fig. 4e, Supplementary Fig. 14d).

Iron in blood deoxyhemoglobin is paramagnetic, thus increasing tissue magnetic susceptibility in the presence of hemorrhage[25]. Using 3D spoiled-gradient-recalled (SPGR) sequence to measure magnetic properties, the edematous areas of *Thbs4^{KO/KO}* animals showed both faster image-intensity decay, and faster R_2* relaxation rate (rate of decay) as compared to littermate controls (Fig. 4d, Supplementary Fig. 14c). *Thbs4^{KO/KO}* animals exhibited significantly increased areas of magnetic susceptibility in the injured cortex as compared to the uninjured contralateral side, while control animals showed only well-defined hyperintense boundaries surrounding the resolving cortical lesions (Fig. 4d, f, Supplementary Fig. 14c, e). While we did not detect these magnetic property differences early on at 2 dpi between control and *Thbs4^{KO/KO}* animals (data not shown), the faster R_2* rate and increased magnetic susceptibility in *Thbs4^{KO/KO}* animals at the later time point indicated presence of extensive, unresolved hemorrhage in their injured cortical regions.

Cortical vasculature compromise can be detected by using biotinylated fixable dextran as tracer[26]. We perfused animals 7 dpi wisth biotinylated dextran and examined their injuries by fixed brain sections. GFAP antibody staining showed that while cortical glial scars can be readily identified in littermate controls, they were poorly defined in *Thbs4^{KO/KO}* animals (Fig. 4g, Supplementary Fig. 12c). Furthermore, whereas biotinylated dextran was largely retained inside the vasculature adjacent to injured areas in littermate controls, in *Thbs4^{KO/KO}* animals we detected widespread parenchymal biotinylated dextran next to the injury sites (Fig. 4g, h). These results are consistent with the MRI analyses above, and indicate continued microvascular bleeds after cortical injury.

Our findings revealed a surprising outcome where SVZ-mediated astrogenesis may be beneficial over neurogenesis in a period after cortical injury, in agreement with potentially protective roles for astrocytes during recovery process in the spinal cord[27]. Furthermore, we believe these results will have important implications for therapeutic interventions using transplanted and/or endogenous NSCs after brain injury[28,29], as well as astrocytic tumors that can arise from the SVZ niche[30].

Full Methods

Cell Culture

Adherent SVZ primary cultures were isolated and grown as described[31]. Cortical astrocyte cultures were grown as described[32]. Jagged1-Fc (R&D Systems) was plated at 5 μg/ml in PBS overnight to coat culture dish surfaces, followed by PBS washes. Recombinant Thbs4 (3 μg/ml, C. Eroglu), DAPT (5 μM, Tocris), DBZ (5 nM, Millipore) were freshly added to culture medium every other day during in vitro differentiation where indicated. Dynasore[33] (Sigma) was used at 30 μM in culture medium.

Immunohistochemistry and live-imaging analyses

Preparation of brain tissue for immunohistochemistry (IHC) was as described[10]. For Thbs4 and DAB staining: after transcardiac perfusion, brains were removed, postfixed overnight, and cryoprotected in 30% sucrose at 4°C. 30 μm coronal sections were serially cut, and immediately incubated for 1 hr at room temperature (RT), floating in PBST blocking buffer containing 10% donkey serum. Primary antibody incubation was carried out at 4°C in blocking buffer overnight, followed by washes in PBST ×3, PBS alone ×3, and secondary antibody incubation in blocking buffer for 2 hrs at RT. DAB staining was carried out according to manufacturer instructions (Vectastain ABC Kit, Vector Labs). For cell counting and quantifications, IHC stained coronal sections, 90 μm apart, starting at the anterior portion of the anterior commissure through the septofimbrial nuclei, were analyzed and counted. Primary antibodies against the following antigens were used: Thbs4 (goat, 1:200, R&D Systems); GFP (chicken, 1:500, Aves Labs); RFP (rabbit, 1:1000, Rockland); GFAP (mouse, 1:2000, Sigma); Mash1 (mouse, 1:100, BD Biosci) DCX (guinea pig, 1:200, Millipore); NeuN (mouse, 1:500, Millipore); Notch1 (rabbit monoclonal EP1238Y, 1:500, Epitomics); Olig2 (rabbit, 1:800, Millipore); NG2 (mouse, 1:200, R&D Systems). Biotinylated fixable dextran (MW = 10 kDa, 1.0 mg/ml, Invitrogen) experiments and their image analyses were performed as described[26]. Live-imaging of migrating neuroblasts was performed as described[34]. All fluorescent images were acquired on Leica TCS SP5 confocal microscope, with control and experimental samples imaged under identical settings.

FACS sorting and gene expression analyses

Cortical and SVZ tissues from *GFAP-GFP* animals (JAX #003257) were dissected in warm NSC culture media[31], dissociated in Neural Tissue Dissociation Kit (Miltenyi) according to manufacturer's protocol. Cell suspension was added to FACS tube on ice, sorted on BD FACS DiVa sorter, followed immediately by Trizol RNA extraction. 500 ng of total RNA was used for cDNA synthesis using SuperScript VILO cDNA Synthesis Kit (Invitrogen). Quantitative PCR analyses were performed as described[35], using the following DNA primers: Thbs4 F: 5′-atccctgctatccaggtgtg-3′, R: 5′-ggcagctcctttcagtcttg-3′; Nfia F: 5′-ccagccagccaagtgaag-3′, R: 5′-gctcagtcacactgaaaacacc-3′; housekeeping gene controls GAPDH F: 5′-catggccttccgtgttcct-3′, R: 5′- tgatgtcatcatacttggcaggtt-3′, and PPIA F: 5′-cgagctctgagcactggag-3′, R: 5′-gatgccaggacctgtatgct-3′. Consistent results were obtained using either housekeeping primer sets.

SDS-PAGE and immunoblotting

Protein extract preparation and Western blotting were performed as described[4]. NIH ImageJ software was used for quantification analyses. Primary antibodies against the following antigens were used: Thbs4 (goat, 1:500, R&D Systems); Thbs2 (mouse, 1:500, Millipore); DCX (guinea pig, 1:1000, Millipore); NICD/Notch1 (rabbit EP1238Y, 1:1000, Millipore); Nfia (rabbit, 1:2000, Active Motif); actin (mouse, 1:5000, Abcam). For pull-down experiments, purified recombinant Thbs4 or Thbs2 (R&D Systems) was incubated for 1 hr at 37°C with either 200 ng mouse Notch1-FC chimera (R&D Systems, 5267-TK) or mouse IgG2a isotype control (Abcam) in Dulbecco's PBS + 1% BSA, 0.1% Triton X-100. Protein G-coupled DynaBeads (Invitrogen), pre-blocked in DPBS + 3% BSA, were then added for 10 min at 37°C, followed by 5 washes in DPBS + 0.1% Triton X-100, and analyzed by Western blotting. For cultured cells, media with or without Thbs4 (3 μg/mL) were first added for 4 hours, washed 2 times with cold PBS, followed by addition of lysis buffer (50mM Tris pH 8.0, 75mM NaCl, 1mM EDTA, 5% sucrose, 0.25% Triton x-100, mini-complete protease inhibitor cocktail), sonication, and centrifuged for 10 minutes at 4°C. Lysates were pre-cleared with Protein A agarose beads (Roche). Rabbit anti-Notch1 antibody (5 μg, Millipore EP1238Y) was added to 1 ml of lysate and incubated overnight at 4°C, followed by addition of Protein A agarose beads, washes as described above, and Western blotting analysis. SVZ IP experiments were performed as described[10] with following modifications: CHAPS lysis buffer contained 5mM CHAPS, 50 mM Tris (pH 7.4), 150 mM NaCl, 1 mM CaCl, 5% sucrose, 0.5% Triton X-100, protease inhibitor cocktail (Roche) + sodium orthovanadate. Supernatants after lysis were subject to two rounds of pre-clearing with BSA-blocked Protein G agarose beads (Roche) for 1 hr each, followed by incubation with rabbit anti-Notch1 antibody (Millipore EP1238Y) for 1 hr, and overnight incubation with BSA-blocked Protein G agarose beads, all at 4°C. Beads were washed five times in lysis buffer, three times in PBS prior to suspension in sample buffer for Western blotting.

Cortical injury and in vivo injections

Photothrombosis cortical injury was performed as described[36]. Briefly, animals were anesthetized and body temperature maintained at 37°C with recirculating water heating pad. Saline solution of rose bengal photosensitive dye (10 mg/ml in saline, 0.1 mg per gram of body weight) was delivered intraperitoneally. Midline scalp incision was made to expose the skull. As external light source, Zeiss KL 1500 LCD (light intensity at 5, 6-minute duration) with 2.5 mm opening light guide was used to induce photothrombosis. Transplantation of passage 2 primary adherent SVZ culture was performed as described[4]. 13 out of 37 transplanted animals showed successfully grafted tdTomato+ cells on analyses. Tamoxifen (10 mg/ml, freshly dissolved in corn oil) was injected intraperitoneally at 0.15 mg per gram of body weight to induce CreER-mediated recombination. All mouse experiments were performed according to approved protocol by IACUC at Duke University.

Magnetic resonance imaging and analyses

Pairs of injured *Thbs4*$^{KO/+}$ and *Thbs4*$^{KO/KO}$ mice were scanned on 9.4 Tesla (400 MHz) 89-mm vertical bore MRI scanner (Oxford Instruments) with shielded coil providing gradients

of 2200 mT/m. Mice were perfused with 10% buffered formalin as previously described[37], followed by overnight fixation in formalin and 3 day incubation in PBS before imaging. All brains were kept within the cranium to prevent potential damage by removal. Diffusion-weighted images (DWI) were acquired using 3D spin-echo sequence with following parameters: field of view (FOV) = $22\times11\times11$ mm^3, matrix = $164\times82\times82$, TE = 12 ms, TR = 2500 ms. One image volume was acquired without diffusion weighting, and diffusion weighting was achieved by applying two half-sine gradient pulses around the 180° refocusing pulse. To produce isotropic weighting, six non-collinear diffusion encoding directions were used at b-value = 3000 s/mm^2. A diffusion tensor was fitted using seven image volumes and mean diffusivity was calculated as described[38]. To examine intracranial hemorrhage, brains were scanned using 8-echo 3D spoiled-gradient-recalled (SPGR) sequence with the following parameters: FOV = $22\times11\times11$ mm^3, matrix = $512\times256\times256$, initial TE = 4.4 ms, echo spacing = 4.9 ms, TR = 100 ms, flip angle = 45°. R_2* relaxation rate was fitted with exponential decay curve. Tissue magnetic susceptibility was quantified as described[39]. Regions of infarct and edema were segmented out based on Mean Diffusivity maps generated via FSL software (Oxford University), and comparable regions in the contralateral uninjured cortex were drawn as references. For each region, Mean Diffusivity, R_2* relaxation rate, and Magnetic Susceptibility were measured. Similar results were obtained with addition of MRI contrast agent ProHance (Bracco Diagnostics, Princeton, NJ) to formalin fixation (1:9, v:v).

Supplementary Material

Refer to Web version on PubMed Central for supplementary material.

Acknowledgments

References

1. Kriegstein A, Alvarez-Buylla A. The glial nature of embryonic and adult neural stem cells. Annu Rev Neurosci. 2009; 32:149–184. [PubMed: 19555289]

2. Kelsch W, Sim S, Lois C. Watching synaptogenesis in the adult brain. Annu Rev Neurosci. 2010; 33:131–149. [PubMed: 20572770]

3. Ihrie RA, Alvarez-Buylla A. Lake-front property: a unique germinal niche by the lateral ventricles of the adult brain. Neuron. 2011; 70:674–686. [PubMed: 21609824]

4. Paez-Gonzalez P, et al. Ank3-dependent SVZ niche assembly is required for the continued production of new neurons. Neuron. 2011; 71:61–75. [PubMed: 21745638]

5. Lawler J, et al. Identification and characterization of thrombospondin-4, a new member of the thrombospondin gene family. J Cell Biol. 1993; 120:1059–1067. [PubMed: 8432726]

6. Eroglu C. The role of astrocyte-secreted matricellular proteins in central nervous system development and function. J Cell Commun Signal. 2009; 3:167–176. [PubMed: 19904629]

7. Deneen B, et al. The transcription factor NFIA controls the onset of gliogenesis in the developing spinal cord. Neuron. 2006; 52:953–968. [PubMed: 17178400]

8. Adams JC, Lawler J. The thrombospondins. Cold Spring Harb Perspect Biol. 2011; 3:a009712. [PubMed: 21875984]

9. Liauw J, et al. Thrombospondins 1 and 2 are necessary for synaptic plasticity and functional recovery after stroke. J Cereb Blood Flow Metab. 2008; 28:1722–1732. [PubMed: 18594557]

10. Kuo CT, et al. Postnatal deletion of Numb/Numblike reveals repair and remodeling capacity in the subventricular neurogenic niche. Cell. 2006; 127:1253–1264. [PubMed: 17174898]

11. Frolova EG, et al. Thrombospondin-4 regulates vascular inflammation and atherogenesis. Circ Res. 2010; 107:1313–1325. [PubMed: 20884877]

12. Merkle FT, Mirzadeh Z, Alvarez-Buylla A. Mosaic organization of neural stem cells in the adult brain. Science. 2007; 317:381–384. [PubMed: 17615304]

13. Thored P, et al. Persistent production of neurons from adult brain stem cells during recovery after stroke. Stem Cells. 2006; 24:739–747. [PubMed: 16210404]

14. Givogri MI, et al. Notch signaling in astrocytes and neuroblasts of the adult subventricular zone in health and after cortical injury. Dev Neurosci. 2006; 28:81–91. [PubMed: 16508306]

15. Li L, et al. Focal cerebral ischemia induces a multilineage cytogenic response from adult subventricular zone that is predominantly gliogenic. Glia. 2010; 58:1610–1619. [PubMed: 20578055]

16. Maxwell KA, Dyck RH. Induction of reproducible focal ischemic lesions in neonatal mice by photothrombosis. Dev Neurosci. 2005; 27:121–126. [PubMed: 16046845]

17. Aguirre A, Rubio ME, Gallo V. Notch and EGFR pathway interaction regulates neural stem cell number and self-renewal. Nature. 2010; 467:323–327. [PubMed: 20844536]

18. Morrison SJ, et al. Transient Notch activation initiates an irreversible switch from neurogenesis to gliogenesis by neural crest stem cells. Cell. 2000; 101:499–510. [PubMed: 10850492]

19. Han H, et al. Inducible gene knockout of transcription factor recombination signal binding protein-J reveals its essential role in T versus B lineage decision. Int Immunol. 2002; 14:637–645. [PubMed: 12039915]

20. Carlen M, et al. Forebrain ependymal cells are Notch-dependent and generate neuroblasts and astrocytes after stroke. Nat Neurosci. 2009; 12:259–267. [PubMed: 19234458]

21. Meng H, Zhang X, Hankenson KD, Wang MM. Thrombospondin 2 potentiates notch3/jagged1 signaling. J Biol Chem. 2009; 284:7866–7874. [PubMed: 19147503]

22. Yamamoto S, Charng WL, Bellen HJ. Endocytosis and intracellular trafficking of Notch and its ligands. Curr Top Dev Biol. 2010; 92:165–200. [PubMed: 20816395]

23. Namihira M, et al. Committed neuronal precursors confer astrocytic potential on residual neural precursor cells. Dev Cell. 2009; 16:245–255. [PubMed: 19217426]

24. Moseley ME, de Crespigny AJ, Roberts TP, Kozniewska E, Kucharczyk J. Early detection of regional cerebral ischemia using high-speed MRI. Stroke. 1993; 24:I60–65. [PubMed: 8249022]

25. Patel MR, Edelman RR, Warach S. Detection of hyperacute primary intraparenchymal hemorrhage by magnetic resonance imaging. Stroke. 1996; 27:2321–2324. [PubMed: 8969800]

26. Daneman R, Zhou L, Kebede AA, Barres BA. Pericytes are required for blood-brain barrier integrity during embryogenesis. Nature. 2010; 468:562–566. [PubMed: 20944625]

27. Faulkner JR, et al. Reactive astrocytes protect tissue and preserve function after spinal cord injury. J Neurosci. 2004; 24:2143–2155. [PubMed: 14999065]

28. Robel S, Berninger B, Gotz M. The stem cell potential of glia: lessons from reactive gliosis. Nat Rev Neurosci. 2011; 12:88–104. [PubMed: 21248788]

29. Aboody K, Capela A, Niazi N, Stern JH, Temple S. Translating stem cell studies to the clinic for CNS repair: current state of the art and the need for a Rosetta Stone. Neuron. 2011; 70:597–613. [PubMed: 21609819]

30. Alcantara Llaguno S, et al. Malignant astrocytomas originate from neural stem/progenitor cells in a somatic tumor suppressor mouse model. Cancer Cell. 2009; 15:45–56. [PubMed: 19111880]

31. Scheffler B, et al. Phenotypic and functional characterization of adult brain neuropoiesis. Proc Natl Acad Sci USA. 2005; 102:9353–9358. [PubMed: 15961540]

32. Christopherson KS, et al. Thrombospondins are astrocyte-secreted proteins that promote CNS synaptogenesis. Cell. 2005; 120:421–433. [PubMed: 15707899]

33. Macia E, et al. Dynasore, a cell-permeable inhibitor of dynamin. Dev Cell. 2006; 10:839–850. [PubMed: 16740485]

34. Platel JC, et al. NMDA receptors activated by subventricular zone astrocytic glutamate are critical for neuroblast survival prior to entering a synaptic network. Neuron. 2010; 65:859–872. [PubMed: 20346761]

35. McDowell KA, et al. Reduced cortical BDNF expression and aberrant memory in Carf knock-out mice. J Neurosci. 2010; 30:7453–7465. [PubMed: 20519520]

36. Lee JK, et al. Photochemically induced cerebral ischemia in a mouse model. Surg Neurol. 2007; 67:620–625. [PubMed: 17512331]

37. Johnson GA, Cofer GP, Gewalt SL, Hedlund LW. Morphologic phenotyping with MR microscopy: the visible mouse. Radiology. 2002; 222:789–793. [PubMed: 11867802]

38. Basser PJ, Mattiello J, LeBihan D. MR diffusion tensor spectroscopy and imaging. Biophys J. 1994; 66:259–267. [PubMed: 8130344]

39. Li W, Wu B, Liu C. Quantitative susceptibility mapping of human brain reflects spatial variation in tissue composition. NeuroImage. 2011; 55:1645–1656. [PubMed: 21224002]
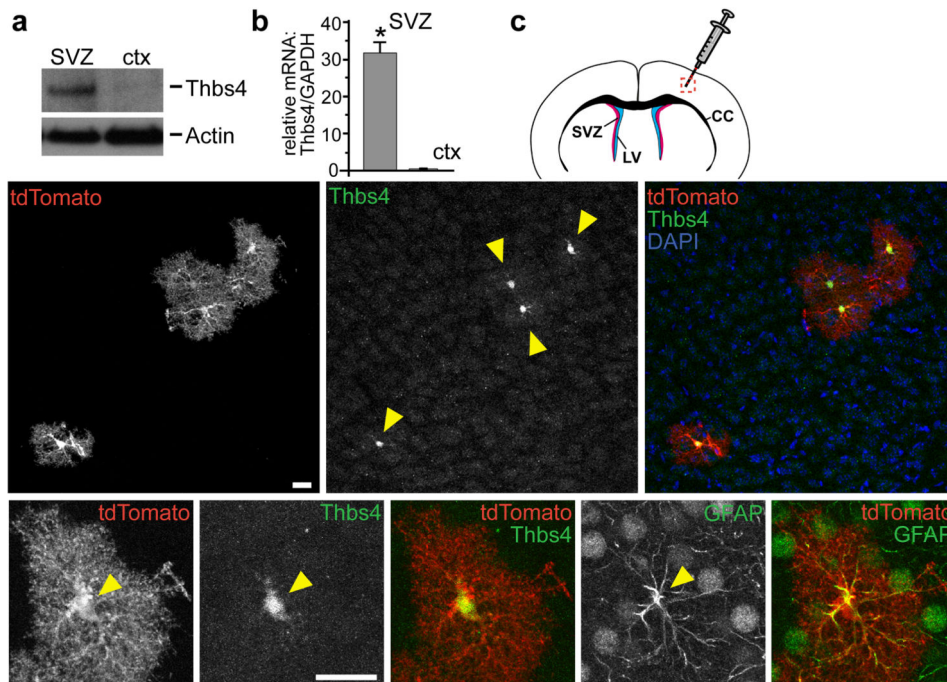
Figure 1. SVZ generation of Thbs4^{hi} astrocytes

a, Western blot analysis of Thbs4 protein levels in differentiated primary SVZ and cortical (ctx) astrocyte cultures. **b**, qPCR analyses of Thbs4 levels in FACS-sorted SVZ vs. ctx GFP$^+$ astrocytes from *GFAP-GFP* transgenic mice, ***** p < 0.001, n = 5, Student's t-test; error bars = sem. **c,** Schematic representation of cortical transplantation strategy. In lower panels, Thbs4, tdTomato, GFAP IHC antibody staining of brain sections, 2-4 weeks after animals were transplanted with lineage-traced primary SVZ NSC cultures derived from tamoxifen-induced *nestin-CreER^{tm}4; r26r-tdTomato* (*N4; RTM*) animals, showing co-localization between tdTomato, Thbs4, GFAP (arrowheads). Scale bar: 20 μm (**c**).
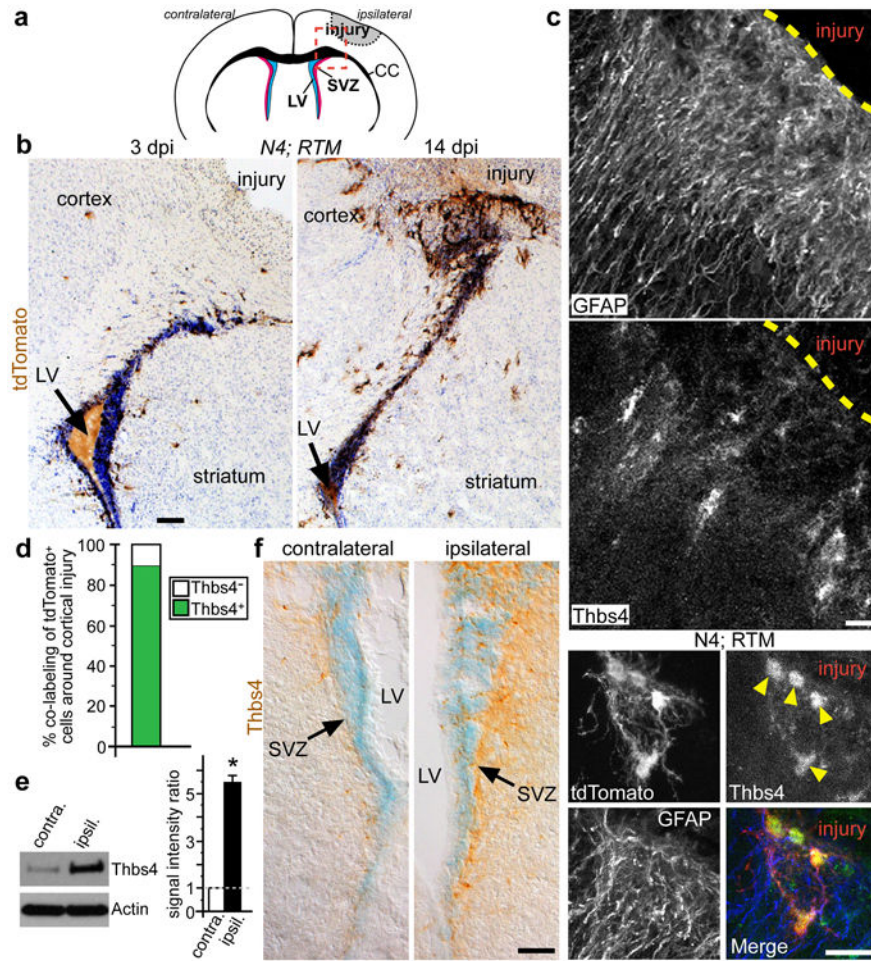
Figure 2. Thbs4^{hi} astrocyte production following photothrombotic cortical injury
a, Schematic representation of photothrombosis injury model, with dashed box indicating region of imaging in (**b**). **b,** DAB IHC staining for tdTomato from *N4; RTM* animals induced with tamoxifen, showing a delayed activation of lineage-traced tdTomato+ cells to injury site 14 dpi. LV = lateral ventricle. **c,** Coronal sections of injury site 14 dpi, IHC stained for GFAP, Thbs4, and tdTomato, showing that lineage-traced tdTomato+ cells adjacent to injury are Thbs4^{hi}GFAP^{+} astrocytes (arrowheads). **d,** Quantitative analyses of total tdTomato^{+} cells at injury site expressing Thbs4 14 dpi (88.10 ± 1.99% stdev, n = 3 animals). **e,** Western blot and quantitative analyses of Thbs4 protein levels in SVZ tissues 3dpi. * p < 0.001, n = 5, Student's t-test, error bar = sem. **f,** DAB IHC staining for Thbs4 expression 3 dpi, Nissl-counterstained. Ipsilateral and contralateral SVZ from the same brain section, imaged under identical conditions. Scale bars: 100 μm (**b**), 20 μm (**c**), 50 μm (**f**).
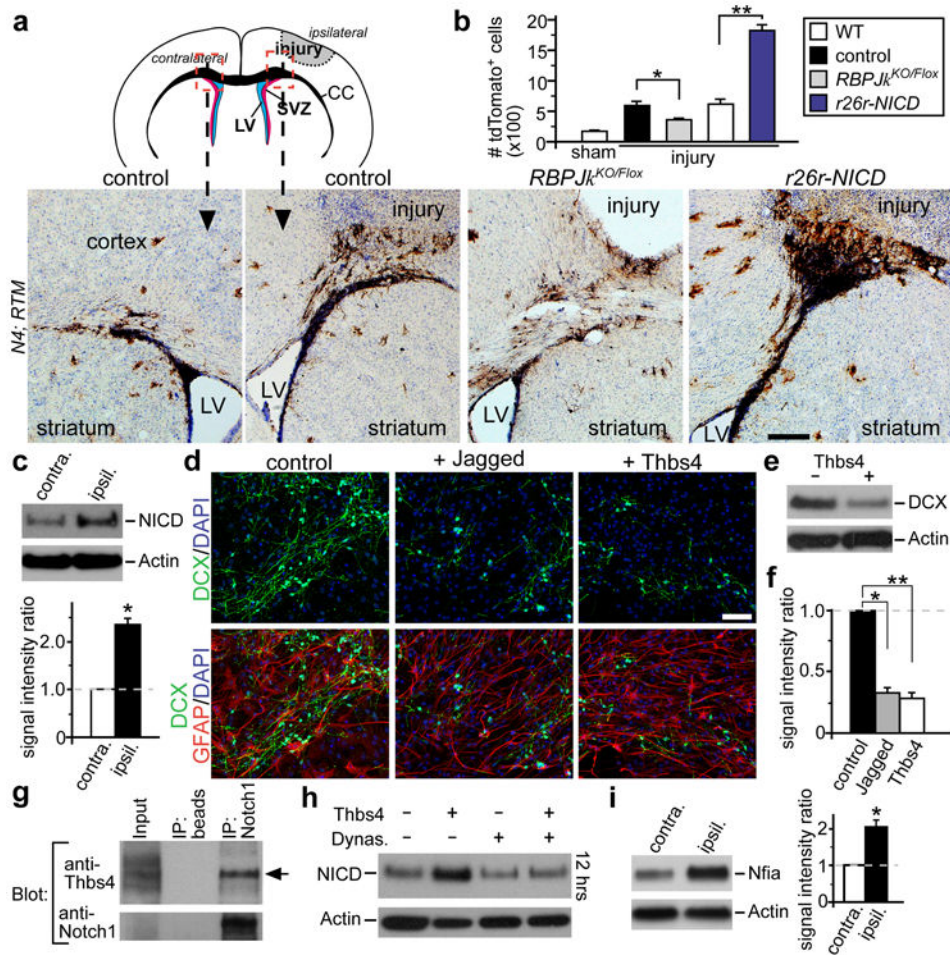
Figure 3. Notch signaling and regulation of injury-induced SVZ astrogenesis
a, Photothrombosis cortical injury model, with areas of imaging indicated by dashed boxes. Representative sections 14 dpi, DAB IHC staining for tdTomato from tamoxifen-induced *N4; RTM; RBPJk$^{Flox/+}$* (control); *N4; RTM; RBPJkKO/Flox* (*RBPJkKO/Flox*); and *N4; RTM; rosa26r-NICD* (*r26r-NICD*) animals. LV = lateral ventricle. **b,** Quantification of tdTomato+ cells above the corpus callosum in each genetic backgrounds 14 dpi, * p < 0.05, n = 6; ** p < 0.001 (WT: n = 8; NICD: n = 5), Student's t-test; error bars = sem. **c,** Western blot analyses of Notch Intra-cellular Domain (NICD) protein levels in SVZ tissues harvested 3dpi, showing upregulation in the ipsilateral over the contralateral side from the same brain. * p < 0.005, n = 5, Student's t-test, error bar = sem. **d,** Differentiation of SVZ adherent neural stem cell cultures, with or without Jagged-Fc, and/or Thbs4 added. **e,** Western blot analyses comparing DCX levels after 5 days of culture differentiation. **f,** Quantification of DCX levels on Western blots. *, ** p < 0.001, n = 5, Student's t-test, error bar = sem. **g,** Freshly isolated SVZ tissue 3 dpi: IP with control beads or anti-Notch1 antibody, and blotted with anti-Thbs4 or anti-Notch1 antibodies, detecting Thbs4 pull-down (arrow). **h,** Thbs4 induction of NICD during in vitro differentiation with or without Dynasore, 12 hrs post stimulation. **i,** Western blot analyses of Nfia levels in SVZ tissues harvested 3 dpi, showing

upregulation in the ipsilateral over the contralateral side from the same brain. ***** p < 0.005, n = 5, Student's t-test, error bar = sem. Scale bars: 200 mm (**a**), 50 μm (**d**).
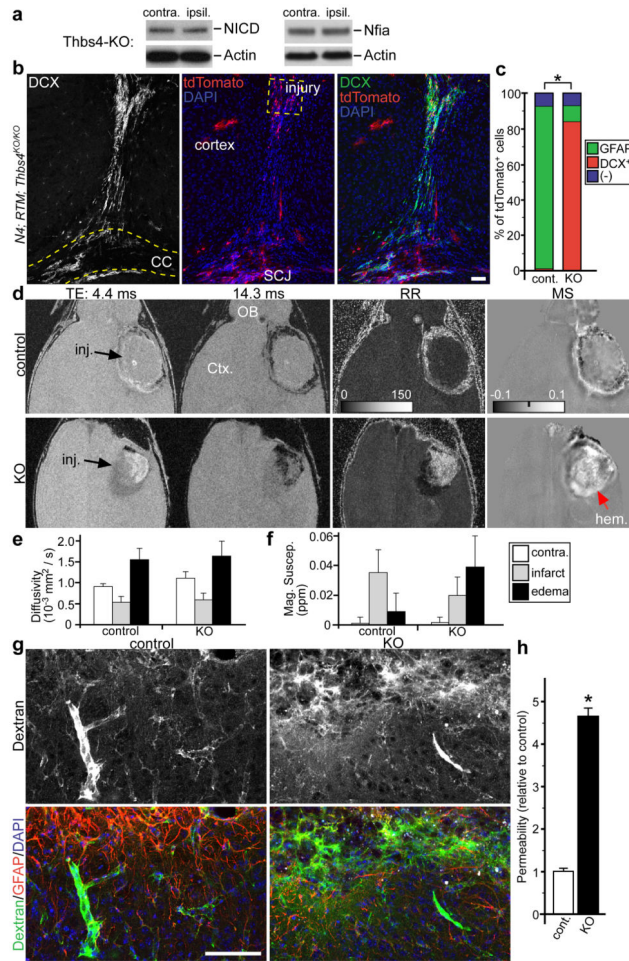
Figure 4. SVZ astrogenesis defects in Thbs4 mutant mice after cortical injury

a, Western blot analyses of NICD and Nfia protein levels in SVZ tissues harvested 3 dpi from Thbs4-KO animals, showing lack of upregulation in the ipsilateral (ipsil) vs. contralateral (contra.) SVZ. **b,** IHC staining for tdTomato, DCX expression from P6 tamoxifen-induced *N4; RTM; Thbs4KO/KO* animals 14 dpi. Note robust DCX+ cells at injury site. SCJ = striatal-cortical junction, CC = corpus callosum (yellow dashed-lines). **c,** Quantification of total tdTomato+ cells around injury site 14 dpi, co-labeling with GFAP or DCX. Lack of strong staining for either GFAP or DCX was marked as (-). ***** $p < 0.002$, n = 11 animals (control), 5 animals (KO), Wilcoxon Rank Sum test. **d,** MRI analyses of littermate pair, *Thbs4KO/+* (control) and *Thbs4KO/KO* (KO) 8 dpi. Left panels = SPGR images, horizontal plane, at two echo times (TE, 4.4 and 14.3 ms). Center panels = computed R_2* relaxation rate (RR). Right panels = corresponding Magnetic Susceptibility (MS). Hyperintense MS indicates area of hemorrhage (hem., red arrow). Scale bar units in RR = s^{-1}, MS = ppm. OB = olfactory bulb, Ctx = cortex, inj = injury site. **e**, **f,** Quantitative measurements of Mean Diffusivity, Magnetic Susceptibility (Mag. Suscep.), comparing contralateral cortex (contra.) to areas of infarct and edema caused by injury. Error bars = stdev. **g,** IHC staining of brain sections 7 dpi to visualize GFAP$^+$ astrocytes and biotinylated dextran infused through vasculature. Extra-vascular biotinylated dextran is readily seen

around cortical injury site in KO animals (close-ups from corresponding dashed-boxes in Supplementary Fig. 12c). **h**, Quantification of parenchymal biotinylated dextran fluorescence next to injury site. ***** $p < 0.001$, n = 5, Student's t-test; error bars = sem. Scale bars: 50 μm (**b, g**).